



3D Model for Representation and Visualization of Magnetic Resonance Spectroscopy Data

Sylvain Gerbaud^{1,3} , Sebastien Horna^{1,3} , Rita Zrour^{1,3} , Carole Guillevin^{2,3} , Mathieu Naudin^{2,3} 
Philippe Meseure¹ 

¹XLIM laboratory, UMR CNRS 7252, University of Poitiers, France, author@univ-poitiers.fr

²LMA laboratory, UMR CNRS 7348, University of Poitiers, France, author2@chu-poitiers.fr

³ I3M, Commun Laboratory CNRS-Siemens, University and Hospital of Poitiers, France,

Corresponding author: Sylvain Gerbaud, sylvain.gerbaud@univ-poitiers.fr

Abstract. Magnetic Resonance Spectroscopy (MRS) is a noninvasive imaging tool providing metabolic imaging to characterize biological tissues. Studies have shown the important role of modeling and visualizing these concentrations according to brain anatomy and in high resolution to improve the study and diagnosis of several diseases such as Alzheimer and tumor. MRS provides information on the relative concentrations of metabolites within a well-localized volume in the brain. This metabolic information is stored inside a single or multiple MRS voxel. Each one of them encompasses several Magnetic Resonance Imaging (MRI) slices and different tissues. However, a voxel only contains a single relative concentration value, which does not take into account distribution and tissue influence. This clinical representation is therefore limited to visualize the impact of the pathology in a fine way. Commonly used software for visualization of these data does not rely on the biological properties of brain tissue to display the metabolite ratio mappings. Thus, its visualization is limited to the resolution of the spectroscopy grid. In this work, we propose a new modeling method that produces a precise model to represent and compute spectroscopic data, based on a reconstruction method offering a 3D topological mesh. The 3D object is then iteratively cut by several planes to extract the part of the mesh included in each MRS voxels. We use this continuous model and the information of the spectroscopy voxel to calculate and visualize the metabolic concentrations in a finer resolution (attached to each anatomical volume).

Keywords: 3D Model of Medical Data, Volumetric Representation and Visualization, Magnetic Resonance Spectroscopy, Corefinement, Topology, Magnetic Resonance Imaging

DOI: <https://doi.org/10.14733/cadaps.2025.430-444>

1 INTRODUCTION

Magnetic resonance spectroscopy (MRS) is a noninvasive technique to explore in vivo biological tissues during brain magnetic resonance imaging (MRI) examination. MRS can give information about the chemical composition of brain tissues, and thus combined with anatomical images, it can be helpful for diagnosis and the following of pathologies (tumors, Alzheimer's diseases, stroke...) [16]. Acquisition can be performed using two different types of sequence: Single voxel spectroscopy (SVS) or multi-voxel chemical shift imaging (CSI). The metabolic information, which is a relative concentration of different molecules, is stored inside a single or multiple MRS voxels, that are precisely localized in the brain [12]. Each voxel encompasses several MRI slices and can be composed of multiple tissues: White matter (WM), gray matter (GM) or cerebrospinal fluid (CSF) at least, and, possibly, different type of lesions due to diseases. Metabolites are known not to be uniformly distributed between anatomical structures. Yet, a single concentration value for each metabolite is given for the whole volume whatever the tissues present in it. This clinical representation is therefore limited to visualize the impact of the anatomical structures in a fine way.

Methodologies have been proposed to improve the accuracy of the acquired values without having to lengthen or complicate clinical protocols. Those are based on the use of partial volume effect (PVE), which gives, for each voxel in a MRI scan, the probability that it belongs to one of the tissue type [3]. Basic interpolation algorithms can be applied on the data in order to improve the spatial resolution of the result. However, the volume composition of a spectroscopy voxel is not taken into consideration. The visualization and representation of concentrations of metabolite dispatch between all different tissues of the brain remains a challenge.

A voxel-based model can be created directly through the segmentation of MRI images, assigning each voxel to a specific physiological element corresponding to an anatomical tissue segment. However, using this discrete representation for modeling brain tissues close to reality exhibits several drawbacks: (1) addressing holes and cavities becomes challenging, (2) the boundaries lack smoothness, and (3) the calculation of geometric properties is constrained by the voxel size. In order to conduct a comprehensive analysis of the anatomical composition of the brain, it is necessary to work with a continuous and coherent 3D mesh. This mesh should consist of compact volumes without overlaps or empty spaces (volumes not associated to any type). A lot of frameworks provide reconstructed (surface) meshes from medical data for precise visualization and analyses [5, 7, 13, 17], mainly based on deep learning algorithms. However, their focus is exclusively on cortical reconstruction, specifically the white matter and pial surface, assuming homomorphism to a sphere. This assumption is flawed in the presence of a tumor or post-operative conditions. Consequently, they lack adequacy in accurately visualizing noisy data comprising multiple tissues representing anatomical elements. Understanding topological relations, such as adjacency and inclusion, is primordial at this stage. This description aligns with the partitioning of 3D space into volumes, incorporating known neighborhood information (topology).

In this paper, we propose a new modeling method that produces a precise model to represent and compute spectroscopic data, based on a reconstruction method offering a 3D topological mesh. The proposed method relies, at first, on a robust, topologically-consistent, volumetric mesh of a brain reconstructed from MRI images, producing a partition of 3D space. The 3D object is then iteratively cut by several planes to extract the part of the mesh included in each MRS voxel. One important point is that, unlike methods that can be found in the literature, this new plane cutting operation explicitly handles the inclusion of volumes during the cut phase. The new topological model is enhanced by spectroscopic data, and then used to better calculate and visualize the metabolic concentrations by exploiting information of each anatomical volume.

All statistics presented in the following have been produced on an Intel core(TM) i9-9900 3.10 GHz processor, with 8 cores and 96 GB of memory. Our method was implemented by integrating the kernel of a topological modeler *Moka* [21] within the open-source software 3D Slicer [9], which provides many tools to analyze and handle medical data.

2 STANDARD MODELING APPROACH

In this section, we introduce the current approach for visualizing the concentration of a metabolite in individual voxels within a well-defined grid in the brain. This grid is specifically localized to the region where the spectroscopic data acquisition took place. Practitioners use both segmented MRI images and MRS grid to visualize a specific metabolite concentration (Figure 1c).

In medical imaging, segmentation is a technique used to isolate and highlight a tissue, lesion, or organ from images, by separating them into different segments. Medical segmentation is represented in the form of a grid of voxels, similar to 3D imaging, where each voxel is assigned a numerical value corresponding to the label of a tissue, enabling them to be distinguished (Figure 1c). This voxel grid is overlayable with that of the MRI images, and thus depends on the dimension and orientation of the latter. In this study, the segmentation grid is created using the FSL-FAST method [23], a widely employed tool for segmenting T1-weighted brain MRI images into distinct tissue categories, including white matter (WM), gray matter (GM) or cerebrospinal fluid (CSF). This method also enables the generation of probability maps for each tissue (PVE). A threshold is then applied to each tissue probability map, leading to the creation of binary masks for each type of tissue. All are combined inside the same grid to produce the segmentation grid, wherein the value of each voxel provides information regarding its belongingness to a tissue (1 for CSF, 2 for WM, 3 for GM with FSL-FAST), or background (value 0). The resolution of the voxel in 3T scans (use for MRS analysis for the brain) depends on the acquisition parameters, but is typically $0.89 \times 0.89 \times 0.9 \text{ mm}^3$ or $1 \times 1 \times 1 \text{ mm}^3$.

MRS acquisition grid is composed of large voxels, in a well-localized volume in the brain. The relative molecular concentration of various metabolites is estimated for each voxel after the acquisition process (Figure 1a). This lower spatial resolution grid, in comparison to MRI images, comprises a substantial volume of voxels, where each one usually measures $6.875 \times 6.875 \times 20 \text{ mm}^3$. Within each voxel, the concentration value is uniformly distributed across its entire 3D space. The practical limitations of available scan time impose significant constraints on the resolution of this type of data. To mitigate the acquisition time and minimize the emergence of artifacts in the estimated data, the voxel volume is increased. Acquiring molecular concentrations with larger voxel sizes enables a reasonable acquisition time for the patient but compromises the analysis of tissue microstructural features [2].

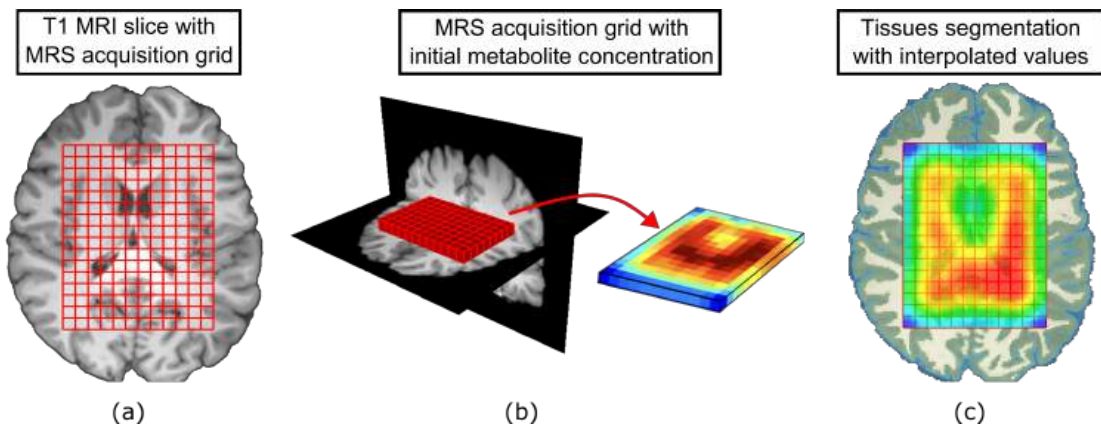


Figure 1: Basic Visualization Method: (a) MRS grid [red colored] on a T1 MRI slice; (b) 3D view of the acquisition grid into the brain and the concentration distribution inside it, from the higher concentration [red colored] to the lower concentration [dark blue colored]; (c) linear interpolation on the estimated concentration values on a MRI slice segmented into three brain tissues: cerebrospinal fluid [blue colored], white matter [white colored] and gray matter [green colored].

The spectroscopic resolution is significantly less refined compared to the resolution used in MRI. Thus, traditional interpolation methods found in typical processing tools rely on interpolation algorithms directly on the images without considering the composition of the brain (Figure 1b) to improve the resolution and detail of the originally acquired data. These approaches are referred to as super-resolution technique, but they do not fix the issue related to PVE and can introduce error when quantifying molecular concentration [14]. Additionally, since the thickness of the acquisition grid consists of a single voxel, interpolation is conducted solely in 2D. These algorithms overlook the heterogeneity within a volume composed of various tissues, potentially resulting in inaccuracies when quantifying metabolite concentrations in smaller voxels. It is possible to work only with a discrete model, but this implies oversampling the coarser grid in order to work with a resolution compatible with both grids [1]. Nevertheless, additional considerations include the fact that MRI and MRS grids cannot be naturally superimposed, either because the MRS grid is not aligned with the MRI images, or because of the size of the voxels, one not being a multiple of the other. In this scenario, an approach using a 3D mesh corresponding as closely as possible to the anatomical data would be more suitable than voxel-based approaches.

3 OUR NEW MODELING METHOD

In order to employ a continuous model for analyzing spectroscopic data, we divide our new modeling approach into two steps: firstly, reconstructing topologically all anatomical tissues from segmented MRI images, and secondly, performing a plane-cutting operation to extract the spectroscopic grid from the mesh. The goal is to generate a more precise and suitable representation of a well localized volume within the brain for medical applications.

3.1 Topological Representation

The first step of the proposed method consists in producing a 3D model that corresponds to the anatomical images. For that purpose, it's crucial to employ a topologically-based model that satisfies specific criteria. Topological data structures, specifically cellular models, delineate the neighbor relationships among cells (vertices, edges, faces, volumes), facilitating efficient processing of the model. Typically, these structures segregate the topological and geometric aspects. Furthermore, a topological model can accommodate various dedicated data such as semantic information, property values or even geometry (coordinates of vertices are usually in \mathbb{R}^3). Our primary goal is to portray anatomical tissues as volumes, ensuring they possess characteristics like being watertight, closed, and having clear adjacency relationships. Moreover, two tissues cannot occupy the same location and the whole space is filled, leading to a space partition. The topological model outlined in this article utilizes Generalized Maps (G-maps) [15], which explicitly represent neighbor relations for all cell dimensions. A 3-G-map defines the structure, or topology, of an object by specifying its boundaries in each dimension: a volume is delineated by its faces, a face by its edges, and an edge by its vertices. The basic element of a G-Map is the **dart**. From now, topological relations in dimension i are denoted α_i . Figure 2 shows how this topology is organized (for clarity, vertices linked in dimension 0 to make up edges are not represented). Also, two darts linked by α_1 represents a vertex (red circles in Figure 2).

For that purpose, a topological 3D reconstruction from the segmented MRI images of the brain tissues is performed based on [10]. The topological reconstruction process consists of two main steps. Initially, using a Marching Cubes (MC) based method [18], we extract the surface corresponding to each segment from the segmented MRI images. As detailed in section 2, the segmentation voxel grid assigns a value to each voxel: 0 for background voxels and a specific number for segmented regions. A black-and-white grid is generated for each segment to indicate voxel membership. Consequently, the resulting surface for each segment represents the isosurface associated with isovalue 0.5, represented by the set of points $X \in \mathbb{R}^3 : F(X) = 0.5$. In the second step, we construct the corresponding G-map to generate topologically closed, watertight volumes. Within

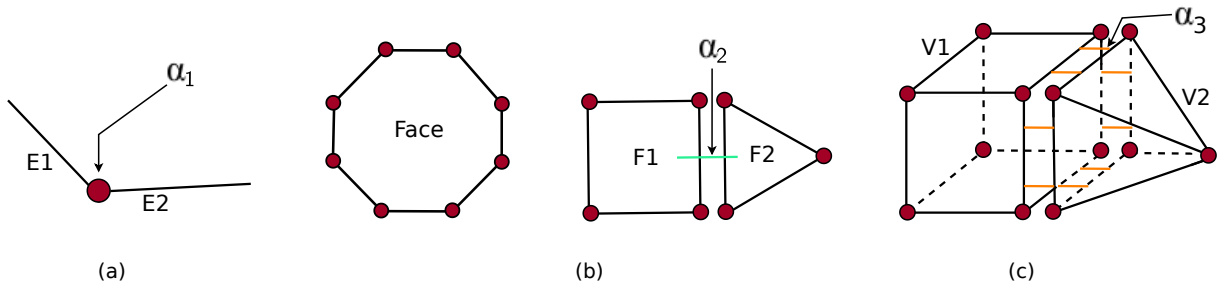


Figure 2: G-Map representation involves connecting topology links α_i in each dimension between cells of the same dimension: (a) edges (dimension 1) connect to form faces, (b) faces (dimension 2) connect to construct volumes, and finally (c) volumes (dimension 3) are linked to create more intricate objects.

these volumes, adjacent faces are explicitly linked at their common edges by topological links of dimension 2 (α_2), illustrated in Figure 2b. Note that inclusion links (volumes completely included in another volume), are not reconstructed. The formalization of the G-Map allows the cells to be associated with semantic information, such as the anatomical tissue from which they come. The geometric, topological and semantic information of the model is used for a multi-criteria classification of the volumes to remove the volumes deemed artifacts in order to respect the anatomical constraints (typically, volumes generated by acquisition noise). Then, all the reconstructed segments are integrated in the same space, by linking the common faces of adjacent volumes of different segments using α_3 links (Figure 2c). Thanks to topological properties, we correct locally all remaining inconsistencies and empty spaces, using PVE maps and anatomical constraints define by our clinical partner (those are optional). Finally, coordinates of each vertex of the 3D mesh are slightly modified using PVE maps in order to deform the model to best match the acquired MRI data. By deforming according to voxel information, we ensure a better adaptation of the constructed shape to the acquired discrete data. Our method automatically produces a partition of the 3D space corresponding to a volumetric mesh from several segmented tissues; in other words, the mesh is free from empty spaces and volume overlaps. This partition exhibits explicit adjacency relationships defined by a G-Map model.

3.2 Cutting by Plane Operation

We aim to cut a 3D mesh according to a spectroscopic grid to obtain a 3D topological spectroscopic model. The resulting model must constitute a partition of space, ensuring that no holes or overlaps are present. To achieve this, we require an operation to separate the elements of a mesh along any given plane while preserving topological coherence and semantic information. Since a grid is a particular mesh, built with infinite planes oriented along three perpendicular directions, it is possible to design a dedicated corefinement process relying on a single operation: the cutting of a mesh by a plane.

Given a soup of faces (volume boundaries), the corefinement operation consists in reconstructing a set of volumes representing the fusion of input meshes, with the necessary adjacency relations, eliminating overlaps and empty spaces by cutting intersecting faces and edges [4]. Aside from self-intersections, the corefinement operation is designed to correct intersections among reconstructed 3D cells (volumes) by operating in lower dimensions (faces and edges). Practical challenges persist, particularly in cutting faces and edges. Exact arithmetic [11] or predicates [24] ensure accuracy but are impractical for large meshes due to resolution time. Various approaches aim to reduce temporal complexity by limiting geometric inaccuracies [6, 8, 20], yet they cannot handle models with nested surface meshes because they do not account for inclusion.

Our method is based on a topological and geometrical process, that deals with volume inclusion and preserves topological and semantic information. Once a cutting plane is defined, we compute its intersection

with the edges of each face and generate *separation lines* representing face/plane intersections.

In the special case where the cutting plane passes through the vertex of a face in the mesh, we consider that the latter is cut out a little before its vertex (using a very small epsilon). This implies that for each face to be cut, whatever the configuration, an even number of intersection points is expected. At each intersection point calculated, a new vertex is inserted into the G-Map. Once the vertices have been inserted, the edges are inserted into the face to split it into two. Indeed, the intersection calculation and, as a consequence the coordinates of the new points to be inserted, are sensitive to numerical precision. Besides, two faces that share a common edge may not position the point of intersection at exactly the same position in space because of a very small offset. To avoid this problem, we rely on the model's adjacency relations, so that an intersection point on an edge of a face is computed only once and used again when an adjacent face is processed (Figure 3). Inserting a vertex automatically affects the incident faces without additional computation time. Once the vertices are inserted, the edges are placed within the face to divide it into two (Figure 4).

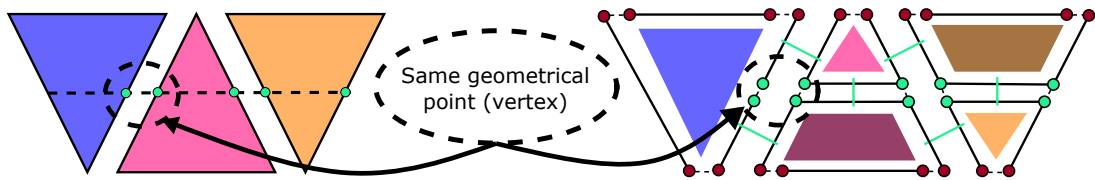


Figure 3: Example of intersection between a separation line and adjacent faces, in compact view (on the left) and its corresponding exploded view (on the right). The newly inserted darts are computed and inserted once, and are depicted in green to differentiate them from those already present before the intersection.

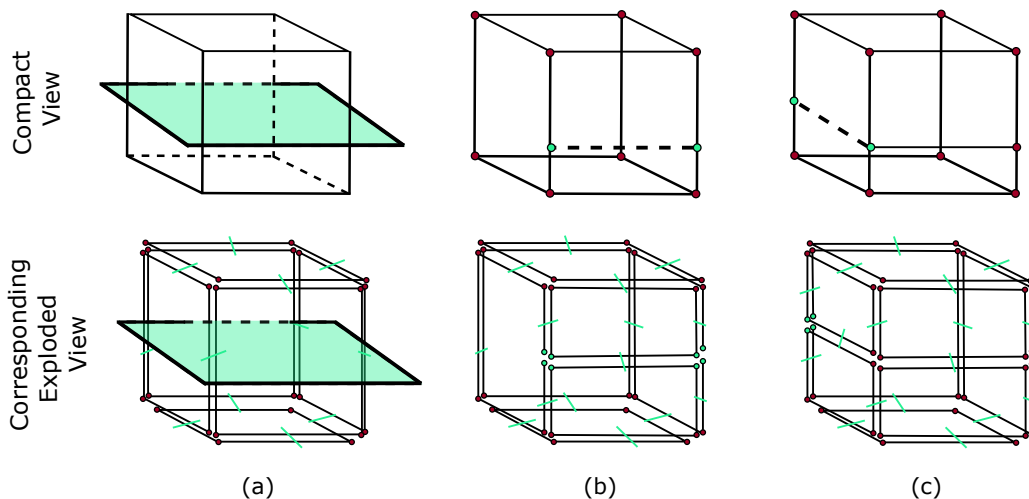


Figure 4: Cutting of only two faces of a cube by a cutting plane (depicted in green) where one face is intersected, and the new darts (highlighted in green, alongside topological edges) are inserted at the intersection point (b), to be utilized again during the cutting of an adjacent face (c).

At this stage, the 3D mesh has not yet been separated according to the cutting plane. To do so, we exploit the intersection points generated by the previous step. The algorithm 1 summarizes the 3 main steps required for generating the cut model.

1. The mesh is first separated based on its new vertices;

2. A closing operation is used to construct the new topological faces, thereby generating the new volumes;
3. An additional closure is applied to these faces in order to maintain the topological properties of the model.

The model is thus properly separated into two at the intersection points inserted according to the cutting plane.

Algorithm 1: Algorithm for generating the cut model from the vertices generated by the intersection point insertion step on the faces

```

Input:  $D$  : The darts created by the intersection/insertion step
1 // ..... Initialization of a list to store pairs of darts.
2  $new\ pairList < dart, dart > ()$  ;
3 // ..... Step 1: unsew the darts to separate the mesh and storing the pairs of unsewn darts.
4 for ( $d \in D$ ) do
5    $pairList.add(d, \alpha_2(d))$  ;
6    $2 - unsew(d)$  ;
7 end for
8 // .....Step 2: Creating new faces by closing the  $\alpha_2$  free darts in  $\alpha_2$ .
9  $2 - closing(D)$  ;
10 // .....Step 3: Sewing in  $\alpha_3$  of each  $\alpha_2$  from the pairs of darts stored in the pair list.
11 for ( $pair \in pairList$ ) do
12    $2 - sew(\alpha_2(pair[0]), \alpha_2(pair[1]))$  ;
13 end for

```

To separate the initial model based on its inserted intersection points, a cut is made according to these points. More precisely, all the new darts are unsewn in α_2 by the topological operation of unravelling in dimension 2. Figure 5 illustrates the cutting generated by this operation. To avoid creating open volumes, two topological closure operation are called to, first, create a face representing the footprint of the cutting plane for each cut volume, and then ensure the property of partition of space. Finally, in case of nested volumes, after the operation is done, co-planar faces may appear. To deal with inclusion information, the newly-created face of the nested volume is included in the one of the container volume. We therefore detect this face inclusion to introduce an inclusion information (as a α_2 link) between the volumes (Figure 6). Semantic information is kept during each part of the process: newly added elements store the semantic of their corresponding volume.

We tested the plane cutting operation on multiple objects, synthetic (models *Sphere* and *Rabbit*) and from data provided by the *3DSlicer* software (the model *BrainS*). The models *Sphere* and *Rabbit* are initially composed of a single volume, with respectively 364 quadrilateral faces and 30,338 triangular faces. Table 1 presents the execution times for the cutting by plane operation applied on these models. The model *BrainS*, on the other hand, consists of 7 volumes and 541,104 faces. For the following tests, the cutting planes were positioned arbitrarily. The mesh complexity, in terms of faces and volumes, plays a significant role on the execution time of each step: the more complex the mesh, the slower the execution time. To reduce the time complexity of the plane cutting operation, we have added an initialization step that examines the model and allows determining the faces that will definitely be cut and working only on those. The variation in time to handle inclusion between cuts 2 and 3 for *BrainS* is due to the addition of inclusion information (Figure 6). In fact, the number of faces to test and their complexity can vary the required processing time for handling inclusion. The plane cutting operation preserved the inclusion of volumes at the cutting level for the *BrainS* model (Figure 6). It can be noted that the number of cutting plane is arbitrary, and will depend of the application (see Section 4).

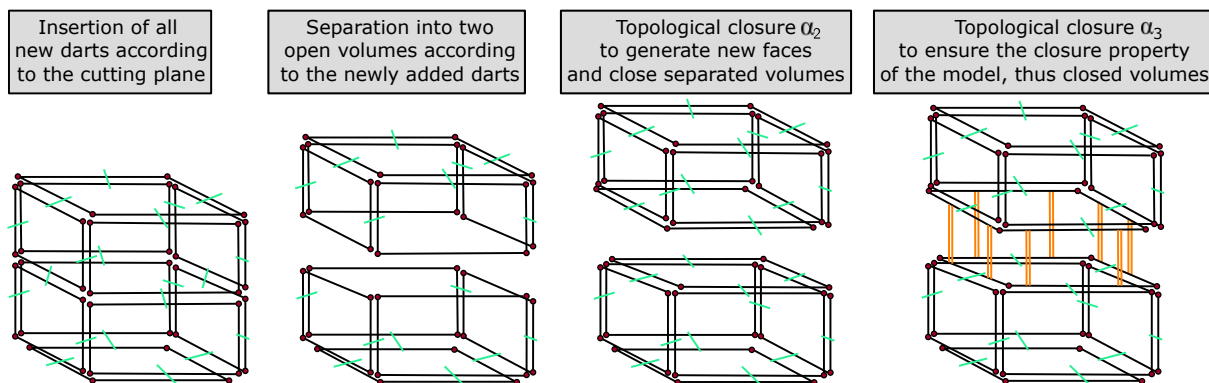


Figure 5: Schematic representation in an exploded view of the separation into 2 closed volumes of a cube by a cutting plane (from Figure 4).

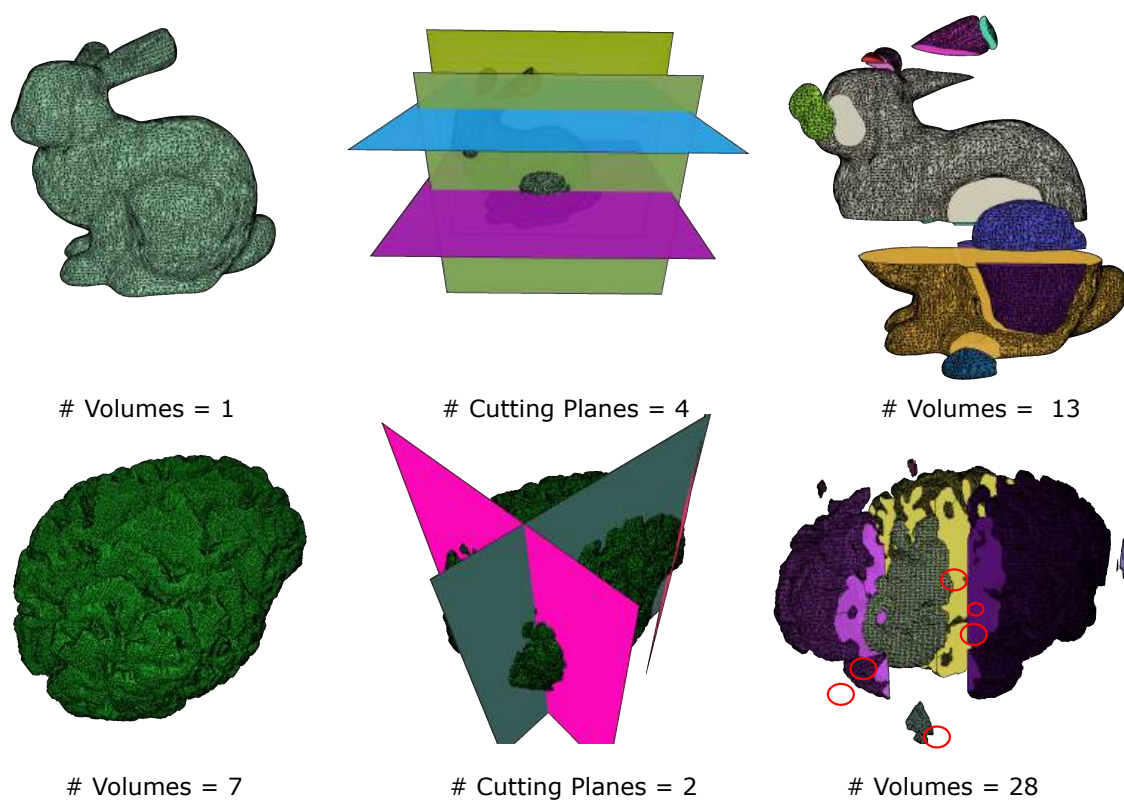


Figure 6: Example of the cutting by plane operation for two different meshes, the results of which, at the right, are in topological view to observe the different volumes generated. From top to bottom: Stanford bunny and a cerebral cortex, which is made up of several nested volumes (inclusion information is encircled in red).

Model	Index of the cut	Initialization time	Insertion step	Separation of the model	Time to handle inclusion
<i>Sphere</i>	1	8ms	1ms	>1ms	7ms
	2	7ms	1ms	>1ms	8ms
<i>Rabbit</i>	1	2s	36ms	79ms	1s
	2	2s	33ms	77ms	1s
	3	1s	38ms	81ms	1s
	4	1s	42ms	86ms	1s
<i>BrainS</i>	1	10s	1s	501ms	17s
	2	12s	2s	224ms	24s
	3	14s	3s	486ms	11s

Table 1: Detailed execution times of the different stages of the cut by plane operation on different models.

Note that, after applying this operation, any part of the mesh that is surely outside the MRS voxel grid can, interestingly, be deleted, even if other plane cuts must still be applied.

4 APPLICATION ON SPECTROSCOPIC DATA

We want to produce a model enriched with topological data that represents the various brain tissues present inside the spectroscopy voxel grid. To achieve this, we apply our new modeling method presented in the previous section 3). The planes used for generating the final model are defined using information about the shape of the grid to be represented (as if we superimposing our model with the voxel grid), thus their number is pre-determined by the acquired grid.

4.1 Generation of the Model

MRI and MRS sequences are performed under the same conditions for a patient. Thus, the anatomical images and spectroscopy voxels are in the same space. Data regarding the placement of images and spectroscopy voxels are stored in the DICOM files output from the acquisition. However, with only MRS data, the voxels cannot be positioned within the anatomical images. Indeed, the coordinates accessible in the DICOM file for MRS acquisition are given in patient space, while MRI images are in image space. Therefore, we need to register the MRS voxels into MRI images.

In practice, MRI information is recorded in the DICOM files output from the machine, and another DICOM file labeled CSI contains the data from the MRS acquisition (in the case of multi-voxel acquisition, otherwise, it would be SVS for a single voxel). In this CSI file, the data is classified according to labels, and we have access to:

- The coordinates of the center of the spectroscopy voxel grid;
- The dimensions and orientation (length, width, and height) of the grid;
- The spacing between two voxel centers along the axes of the three planes (coronal, axial, and sagittal).

We know that a CSI grid consists only of voxels arranged in rows and columns. Their number is derived from the spacing and dimensions of the grid. Since the coordinates of the center of the CSI grid are provided in patient space, we perform a transformation using the MRI image positioning matrix. This allows positioning

this center in the space of the anatomical images, and it is sufficient to exploit this information to find the coordinates of the first voxel of the spectroscopy grid. Thus, we can create the rest of the voxels using the number of rows and columns.

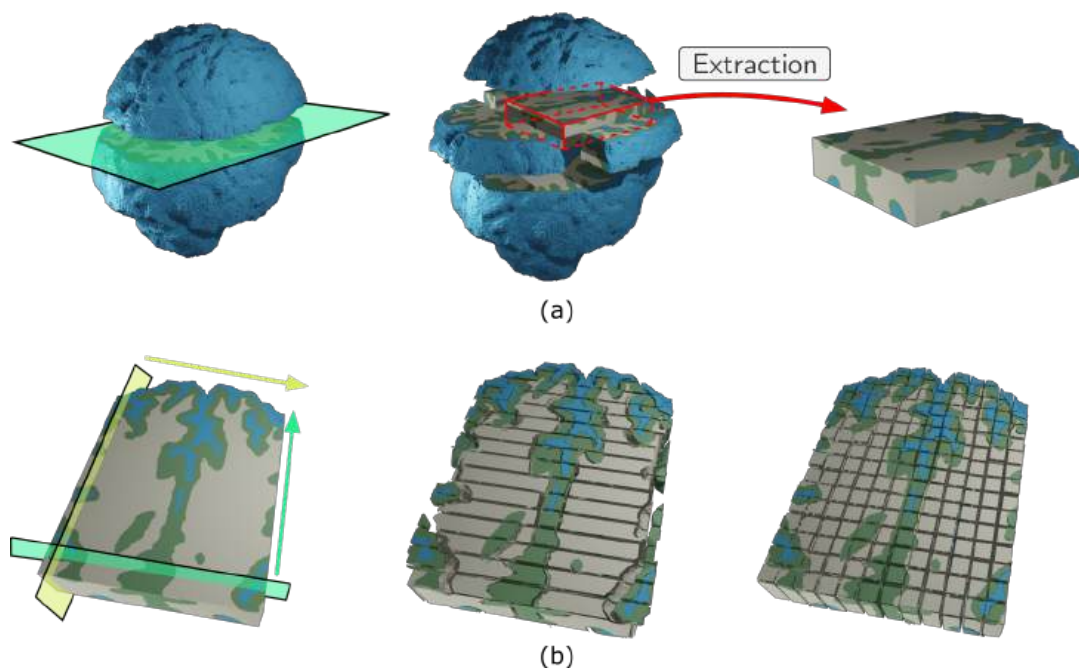


Figure 7: Generation of the 3D model of the spectroscopy voxel grid. (a) 3D view of the first cut on the brain, with volumes separated at the level of the green plane, and after the 6 cuts, extraction of the volumes contained within the MRS grid; (b) successive cuts following the green plane and the direction of the green arrow to represent the lines of the SRM voxel grid, then the same with the yellow one.

The plane cutting operation is used multiple times successively, first to restrict the entire brain model to the area corresponding to the spectroscopy voxel grid and then to produce the final model. Specifically, the plane cutting operation is applied along the x , y , and z axes, twice per axis, using the normals of the faces of the initial grid to define the planes. After each separation of the initial model, the unnecessary part is permanently removed (Figure 7a). This portion removed from the result corresponds to volumes that lie outside the area acquired during the SRM acquisition. From a purely technical standpoint, this also helps reduce the mesh size, thus reducing the temporal complexity of subsequent processing steps, as well as the memory complexity of the model. At this stage, the cuts based on the SRM voxel grid are missing. Therefore, the plane cutting operation is applied successively to obtain the number of columns and rows corresponding to the spectroscopy voxel grid (Figure 7b). From the data acquired by SRM, we can deduce the normal and coordinates of each cutting plane, as well as their number. Figure illustrates the result obtained from the initial data.

At the end of this step, we have a 3D topological model accurately representing the volumes contained within the study area of the SRM acquisition. The model is now ready to be enriched with spectroscopy information. Obviously, tissue semantic information is preserved throughout these steps, and inclusion between volumes of different tissues are taken care explicitly to keep the topological properties of the model.

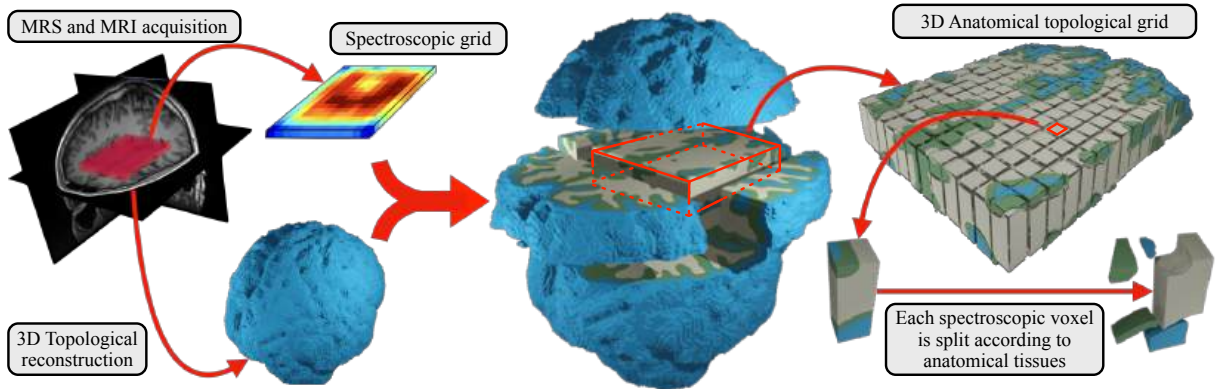


Figure 8: 3D Anatomical topological construction matching the spectroscopy grid. Using the information of the spectroscopy grid and its voxels, the 3D brain model is split in accordance with the number of rows and columns of the initial grid. The resulting model is composed of identified volumes, from a specific spectroscopy voxel and brain tissue.

4.2 Results and Discussion

Applied to the context of MRS, we have a 3D topological model that accurately represents the volumes contained in the study area of the MRS acquisition (Figure 8). This section presents results of our new modeling method on real MRI and MRS scans on a healthy patient (*Healthy*). Images are acquired on a Magnetom Skyra 3 Tesla (Siemens Healthineers, Erlangen, Germany). The sequence used is a 3D T1 MPRAGE 0.9 mm isotropic (TE: 2.41 ms, TR: 1950 ms, TI: 816 ms, FOV: 256 by 213 mm², matrix: 240x288, slices: 192, turbo factor: 224). Original DICOM data are converted to NIFTI to be used in our homemade automated pipeline. As a post-processing step, FSL-BET [19] is applied to remove subcutaneous fat in order to create a mask of brain only. Then, FSL-FAST is launched to obtain the 3 segmentation classes: (i) Cortex also known as Gray Matter, (ii) White Matter, (iii) Cerebral Spinal Fluid.

Table 2 presents the evolution of the number of faces and volumes during the successive plane cutting operation, along with the associated execution time. As a reminder, the modelisation of the 3D topologic spectroscopy grid starts with six cuts (two per axis), and at the end of each of them, the cut volumes deemed unnecessary for the subsequent process are removed. Thus, we observe that the first cut is the one that requires the most time but also eliminates the most volumes. This is partly explained by the fact that the operation processes a larger number of volumes during its execution (a number that then reduces significantly, along with the execution time). In fact, the order of the cuts was not chosen randomly. The first cut aims to eliminate the largest number of volumes and thus reduce the size of the model, and is chosen upstream by studying the number of elements that will possibly be eliminated by the plane cutting operation for a specific plane. Table 3 presents in detail the distribution of the computation time required for the operation for the six cuts. As observed in the previous section 3, initialization time and inclusion handling time are the longer ones, because the number of elements to process affects the duration of these steps of the operation.

We can now enhance the model by spectroscopic information. Since the plane cuts were used to separate the volumes to represent the grid voxels acquired by MRS, each reconstructed volume has the voxel identifier and the initial relative concentration of the metabolite. Also, for each volume in the final model, we know the nature of the associated anatomical tissue (semantics), the identifier of the spectroscopic voxel and the adjacent volumes (topological neighbourhood). Thus it encompasses all necessary information to compute and represent accurate metabolic concentration and dispatch it between every anatomical volume. To give a

Model	Index of the cut	Elapsed time	# initial volumes	# initial faces	# deleted volumes
<i>Healthy</i>	1	3min 47s	835	1 930 522	789
	2	2min 02s	105	1 483 912	69
	3	1min 14s	88	704 546	16
	4	42s	87	661 663	33
	5	38s	78	612 695	23
	6	33s	77	567 077	18

Table 2: Characteristics of the first six cuts of a healthy brain model, in order to restrict the entire brain model to the area corresponding to the spectroscopy voxel grid (Figure 7a).

Model	Index of the cut	Initialization time	Insertion step	Separation of the model	Time to handle inclusion
<i>Healthy</i>	1	1m 18s	9s	4s	2min 16s
	2	40s	6s	2s	42s
	3	20s	1s	1s	30s
	4	18s	1s	1s	22s
	5	16s	1s	1s	20s
	6	14s	1s	1s	19s

Table 3: Detailed execution times of various treatments during the first six cuts of a healthy brain model.

more precise example, the concentration of a metabolite present in a single tissue can be reinterpreted by the actual volume covered by the tissue and not the whole volume of the voxel, so the concentration obtained is higher. The molecular concentration is thus recalculated for each volumes based on mass conservation, the concentration of a given metabolite in each tissue related to its distribution rates, and the exact volume size, more details regarding these calculations can be found in [1]. The topological definition of volumes allows all computations to be performed locally, which greatly reduces the processing time. The study of metabolic concentration inside the brain using our 3D model is shown in Figure 9.

We tested our model on real spectroscopic data to show the variation in the concentration of a metabolite in each tissue on healthy patients. Within distinct volumes, a minor variation in metabolite concentration is noted for identical tissue types. This variation arises from the impact of both the tissue's inherent characteristics and its specific position within the brain on the concentration values [22] and our results correspond to the literature (see Table 4). In comparison, conventional methods yield a consistent concentration value throughout the entire depth of a voxel acquisition for a given 2D position, which does not give information about the impact of a tissue on the metabolism. With our model, we propose two kinds of visualization: within or by discretizing our 3D model. By giving continuous volumes, we offer more details about the changes in metabolic concentration, mainly at the borders between the reconstructed tissues. Also, our model does not contain any ambiguous volumes by exploiting PVE maps during the reconstruction process, compared to voxel-based representation. By discretizing our model, we can produce 2D slices that display a metabolite concentration contain in each corresponding 3D volume. The resolution of the visualization can be chosen arbitrarily by practitioners to facilitate their studies regarding the influence of brain tissue on metabolism. In fact, the resolution can be increased, thus giving higher definition at the boundaries between tissues.

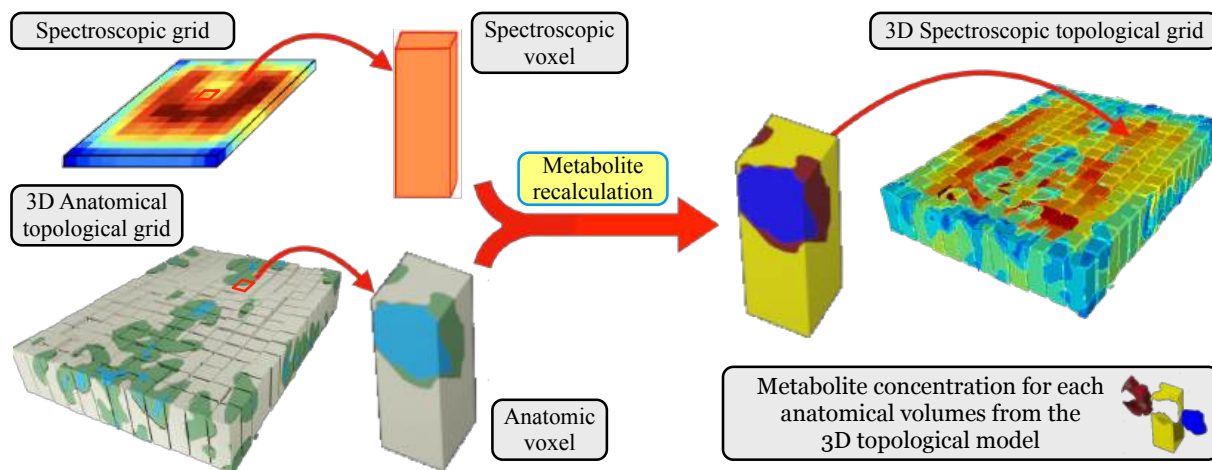


Figure 9: Metabolites computation on the spectroscopy voxel grid: The concentration of a spectroscopy voxel is distributed in an anatomical voxel according to its tissue.

Metabolite	N-acetylaspartate (NAA)		Choline (CHO)		Creatine (Cr)	
	GM region	WM region	GM region	WM region	GM region	WM region
Clinical studies [22]	15.7 ± 1.5	17.6 ± 1.6	1.8 ± 0.4	2.7 ± 0.5	11.3 ± 1.4	10.3 ± 1.2
Our model	15.7 ± 1.4	17.5 ± 1.7	1.6 ± 0.5	2.7 ± 0.6	11.1 ± 1.6	10.3 ± 1.3

Table 4: Quantitative comparison of metabolite concentration (in mmol kg^{-1}) variations between those calculated using our model and those estimated in [22] for several metabolites inside gray matter and white matter.

5 CONCLUSIONS

In this work, we have proposed a new modeling method to produce a model that represent and visualize in a finer way spectroscopic data. Our method apply a specific corefinement process between the acquired MRS grid and the anatomical 3D mesh. The new proposed model ensures that the geometry of the tissue covered by each voxel is well defined and topologically coherent. Using the well-identified volumes, distribution of a metabolite concentration takes into account the real nature of the underlying tissues based on distribution rates evaluated in clinical studies. Our 3D topological model is an adaptive tool to represent anatomical structures and their impact on the metabolism as close as possible to the real data.

ACKNOWLEDGEMENTS

This research is funded by Region Nouvelle-Aquitaine AAPR2020A-2020-8595610, France and SIEMENS Healthineers.

Sylvain Gerbaud, <https://orcid.org/0000-0002-2375-6754>

Sebastien Horna, <https://orcid.org/0000-0002-9170-6513>

Rita Zrour, <https://orcid.org/0000-0002-0733-1326>

Carole Guillevin, <https://orcid.org/0000-0003-1075-4730>

Mathieu Naudin, <https://orcid.org/0000-0001-8778-0297>
 Philippe Meseure, <https://orcid.org/0000-0001-6652-8738>

REFERENCES

- [1] Abd Alaziz Obeid, H.; Zrour, R.; Mercier, B.; Horna, S.; Guillevin, C.; Khalil, M.: 3d modeling for multimodal visualization of medical data, 2023. <http://doi.org/10.14733/cadconfP.2023.195-199>.
- [2] Al-ledani, O.; Lechner-Scott, J.; Ribbons, K.; Ramadan, S.: Fast magnetic resonance spectroscopic imaging techniques in human brain-applications in multiple sclerosis. *Journal of biomedical science*, 24, 1–19, 2017. <http://doi.org/10.1186/s12929-017-0323-2>.
- [3] Ballester, M.A.G.; Zisserman, A.P.; Brady, M.: Estimation of the partial volume effect in mri. *Medical image analysis*, 2002. [http://doi.org/10.1016/S1361-8415\(02\)00061-0](http://doi.org/10.1016/S1361-8415(02)00061-0).
- [4] Belhaouari, H.; ; Horna, S.: Reconstruction of volumes from soup of faces with a formal topological approach. *Computer-Aided Design and Applications*, 2019. <http://doi.org/10.14733/cadaps.2019.972-984>.
- [5] Bongratz, F.; Rickmann, A.M.; Polsterl, S.; Wachinger, C.: Vox2cortex: Fast explicit reconstruction of cortical surfaces from 3d mri scans with geometric deep neural networks. *Proceedings of the IEEE/CVF Conference on Computer Vision and Pattern Recognition*, 2022. <http://doi.org/10.48550/arXiv.2203.09446>.
- [6] Botsch, M.; annd M. Pauly, L.K.; Alliez, P.; Levy, B.: *Polygon mesh processing*. A K Peters/CRC press, 2010. <http://doi.org/10.1201/b10688>.
- [7] Dale, A.; Fischl, B.; Sereno, M.: Cortical surface-based analysis. i. segmentation and surface reconstruction. *NeuroImage*, 9, 179–194, 1999. <http://doi.org/10.1016/j.neuroimage.2012.09.050>.
- [8] Fang, X.; Desbrun, M.; Bao, H.; Huang, J.: Topocut: fast and robust planar cutting of arbitrary domains. *ACM Transactions on Graphics (TOG)*, 41(4), 2022. <http://doi.org/10.1145/3528223.3530149>.
- [9] Fedorov, A.; Beichel, R.; Kalpathy-Cramer, J.; Finet, J.; Fillion-Robin, J.C.; Pujol, S.; Bauer, C.; Jennings, D.; Fennessy, F.; Sonka, M.; Buatti, J.; Aylward, S.; Miller, J.; Pieper, S.; Kikinis, R.: 3d slicer as an image computing platform for the quantitative imaging network. *Magn. Reson. Imaging*, 30, 1323–1341, 2012. <http://doi.org/10.1016/j.mri.2012.05.001>.
- [10] Gerbaud, S.; Horna, S.; Zrour, R.; Naudin, M.; Guillevin, C.; Meseure, P.: Reconstruction and topological cleaning of brain mr images. *Sixth International Conference on Advances in Biomedical Engineering (ICABME)*, 2021. <http://doi.org/10.1109/ICABME53305.2021.9604811>.
- [11] Hu, Y.; Zhou, Q.; Gao, X.; Jacobson, A.; Zorin, D.; Panozzo, D.: Gmp - the gnu multiple precision arithmetic library, 2021. <https://gmplib.org>.
- [12] Jissendi Tchofo, P.; Baleriaux, D.: Brain 1h-mr spectroscopy in clinical neuroimaging at 3t. *Journal of Neuroradiology*, 2009. <http://doi.org/10.1016/j.neurad.2008.04.001>.
- [13] Lebrat, L.; Santa Cruz, R.; de Gournay, F.; Fu, D.; Bourgeat, P.; Fripp, J.; Fookes, C.; Salvado, O.: Corticalflow: A diffeomorphic mesh deformation module for cortical surface reconstruction. In *Advances in Neural Information Processing Systems*, vol. 34, 2021. <http://doi.org/10.48550/arXiv.2206.02374>.
- [14] Lepcha, D.C.; Goyal, B.; Dogra, A.; Goyal, V.: Image super-resolution: A comprehensive review, recent trends, challenges and applications. *Information Fusion*, 91, 230–260, 2023. <http://doi.org/10.1016/j.inffus.2022.10.007>.
- [15] Lienhardt, P.: N-dimensional generalized combinatorial maps and cellular quasi-manifolds. *International Journal on Computational Geometry and Applications*, 4, 275–324, 1994. <http://doi.org/10.1142/S0218195994000173>.

- [16] Melissa, M.; Scott, P.; Timothy, L.: Early alzheimer's disease neuropathology detected by proton mr spectroscopy. *Journal of Neuroscience*, 2014. <http://doi.org/10.1523/JNEUROSCI.2027-14.2014>.
- [17] Santa Cruz, R.; Lebrat, L.; Bourgeat, P.; Clinton, F.; Fripp, J.; Salvado, O.: Deepcsr: A 3d deep learning approach for cortical surface reconstruction. *Proceedings of the IEEE/CVF Winter Conference on Applications of Computer Vision*, 2021. <http://doi.org/10.1109/WACV48630.2021.00085>.
- [18] Schroeder, W.; Maynard, R.; Geveci, B.: Flying edges: A high-performance scalable isocontouring algorithm. *5th IEEE Symposium on Large Data Analysis and Visualization*, 33–40, 2015. <http://doi.org/10.13140/RG.2.1.3415.9609>.
- [19] Smith, S.: Fast robust automated brain extraction. *Human Brain Mapping*, 17, 143–155, 2002. <http://doi.org/10.1002/hbm.10062>.
- [20] Tao, M.; Batty, C.; Fiume, E.; Levin, D.I.: Mandoline: robust cut-cell generation for arbitrary triangle meshes. *ACM Transactions on Graphics (TOG)*, 38, 1–17, 2019. <http://doi.org/10.1145/3355089.3356543>.
- [21] Vidil, F.; Damiand, G.; Dexet-Guiard, M.; Guiard, N.; Ledoux, F.; Fousse, A.; Fradin, D.; Liang, Y.; Meneveaux, D.; Bertrand, Y.: Moka: 3d topological modeler, 2002. <https://projet.liris.cnrs.fr/moka/index.php>.
- [22] Wright, A.M.; Murali-Manohar, S.; Henning, A.: Quantitative t1-relaxation corrected metabolite mapping of 12 metabolites in the human brain at 9.4 t. *NeuroImage*, 2022. <http://doi.org/10.1016/j.neuroimage.2022.119574>.
- [23] Y. Zhang, M.B.; Smith, S.: Segmentation of brain mr images through a hidden markov random field model and the expectation-maximization algorithm. *IEEE Trans Med Imag*, 20, 45–57, 2001. <http://doi.org/10.1109/42.906424>.
- [24] Zhou, Q.; Grinspun, E.; Zorin, D.; Jacobson, A.: Mesh arrangements for solid geometry. *ACM Transactions on Graphics (TOG)*, 35, 1–15, 2016. <http://doi.org/10.1145/2897824.2925901>.